International Journal of Mechanical Sciences 136 (2018) 134–142

Contents lists available at ScienceDirect

International Journal of Mechanical Sciences

journal homepage: www.elsevier.com/locate/ijmecsci

An origami-inspired structure with graded stiffness

Jiayao Ma[a,b,1], Jichao Song[b,1], Yan Chen[a,b,*]

[a] Key Laboratory of Mechanism and Equipment Design of Ministry of Education, Tianjin University, Tianjin 300072, China
[b] School of Mechanical Engineering, Tianjin University, Tianjin 300072, China

ARTICLE INFO

Keywords:
Rigid origami
Functionally graded structure
Self locking
Graded stiffness
Energy absorption

ABSTRACT

Origami-inspired structures and mechanical metamaterials are often made up of individual tessellating repeat units, the folding and relative geometry of which determine the overall mechanical properties. If these units are identical, then the mechanical behaviour of the structure is uniform throughout, meaning that it is not able to adapt to changeable loading conditions. Here we create and study an origami structure, based on the Miura-ori folding pattern, which has a varying geometry over its volume and graded stiffness. Using kinematic analysis, we show how geometric parameters of the folding pattern can be varied to create both rigid foldable and self locking stages. We demonstrate both experimentally and numerically that the structure can achieve periodically graded stiffness when subjected to quasi-static out-of-plane compression, and the mechanical responses can be tuned by changing the underlying geometric design. We obtain a structure with superior energy absorption capability to uniform tessellating repeat units, and anticipate that this strategy could be extended to other structures and metamaterials to impart them with non-uniform and graded mechanical properties.

1. Introduction

Origami has recently seen a surge in research interests from mathematicians, engineers and physicists. Making use of the superior ability of origami to transform 2D sheet materials into complicated 3D shapes, researchers have developed novel structures with a wide range of engineering applications, such as deployable structures [1,2], medical foldable devices [3], energy absorption structures [4–11] and mechanical metamaterials [12–22].

When prefolding a thin-walled structure following a proper origami pattern, its buckling and post-buckling modes can be pre-designed, which leads to a device with low peak force and high energy absorption efficiency. Ma and You [4] applied a novel origami pattern to square tubes in order to induce a complete diamond mode with doubled number of travelling plastic hinges. Quasi-static numerical simulations showed that both low peak force and high energy absorption efficiency were achieved in comparison with those of conventional square tubes. Experimental studies on the dynamic performance [5] and imperfection sensitivity [6] of the origami crash box were also conducted. Kite-shape pattern [7] and Tachi-Miura polyhedron bellows [8] were also adopted in the design of energy absorption devices, and an improvement in energy absorption capacity was obtained. Regarding circular tubes, Yang et al. [9] applied diamond origami pattern in circular tubes and achieved a significantly reduced peak force while the energy absorption was not compromised. Wu et al. [10] studied sinusoidal corrugation tubes and found out that both the initial peak crushing force and fluctuations of force–displacement curve were mitigated by the pattern.

In addition, origami-inspired mechanical metamaterials have gained increasing popularity in the ongoing quest for materials with exotic properties such as negative Poisson's ratio [12–17] and programmable stiffness [18–20]. Schenk and Guest [12] were among the first to propose a Miura-ori [1] based metamaterial and investigated its geometry, density, and Poisson's ratio in details. Lv et al. [13] also studied the geometry of Miura-folded plates and reported that the Poisson's ratio could be positive by varying pattern geometry. Wei et al. [14] conducted a thorough theoretical analysis of the three-dimensional elastic response of a single layer of Miura-ori folded sheet. By stacking Miura-ori sheets, curved origami structures with great morphing capability and self locking response were created [23]. In addition, multi-stable elastic behaviours [24] and structural weight reduction [25] were also achieved. To tune the stiffness of Miura-folded sheets, Silverberg et al. [18] introduced a kind of pop-through defect and obtained the correlation between the in-plane compression stiffness and the number, location, and combination of the defect. Besides, Miura-derivative fold patterns [21] and square twist pattern [22] have also been investigated in the design of origami mechanical metamaterials.

Up to now, most origami structures and metamaterials are formed by repetition of identical pattern unit cells. Those units are either rigid

* Corresponding author at: School of Mechanical Engineering, Tianjin University, Tianjin 300072, China.
E-mail address: yan_chen@tju.edu.cn (Y. Chen).

[1] Joint first authors.

https://doi.org/10.1016/j.ijmecsci.2017.12.026
Received 14 November 2017; Received in revised form 13 December 2017; Accepted 17 December 2017
Available online 18 December 2017
0020-7403/

foldable ones, in which the deformation is only caused by rotation of creases while the panels remain rigid, to take advantage of the mechanism motion during deformation [17], or non-rigid ones to involve global material bending [22]. For a given origami pattern, besides the material selected, the mechanical behaviour is mainly determined by its geometric parameters, and therefore identical unit cells usually lead to uniform structural stiffness. However, under certain circumstances, a graded stiffness could enhance the functionality of metamaterials. For instance, in the design of the body of a transport vehicle which is soft when in contact with a human and but can be very rigid to protect occupants in a crash [26,27], or non-lethal projectiles for crowd control or peace support operations [28], materials with a graded stiffness is advantageous over those with a uniform stiffness. Such functional graded mechanical properties have been widely seen in nature, e.g., bamboos and bones have specifically graded distribution of cell number or cell size to adapt to their expected service environments [29–31]. Man-made functionally graded structures and materials have also been achieved, mainly by means of changing material density [32,33] or thickness [34–36]. However, no origami structure, which is able to systematically achieve graded stiffness through a proper geometric design while still preserving the native folding behaviours of the origami pattern, has been reported. Compared to previous designs with varying density or thickness, such structure can be made out of a single type of sheet materials with a uniform thickness, thereby greatly reducing the manufacturing costs.

Therefore, the objective of this paper is to design an origami structure based on the Miura-ori pattern, which is constructed by unit cells that are geometrically varied over the volume of the material, in order to create graded stiffness and high energy absorption when subjected to quasi-static out-of-plane compression. The layout of the paper is as follows. The geometry of the graded origami structure is first presented in Section 2. Section 3 gives details about the experimental setup and finite element modelling approach that are adopted in the quasi-static compression study of the origami structure. Subsequently are the results and discussions in Section 4. And the conclusion is given in Section 5 which ends the paper.

2. Geometry

2.1. Geometric design

A unit cell of the Miura-ori pattern as shown in Fig. 1(a) is composed of four creases meeting at one point, dividing it into four identical parallelogram panels. It is parameterised by two side lengths a and b, sector angle ϕ, and folding angle θ. The edge angles η and γ, and the dimensions w, l, v, and h can be calculated from the four independent parameters through the following equations [37]

$$\cos\gamma = \frac{\sin^2\phi\cos^2(\theta/2) - \cos^2\phi}{\sin^2\phi\cos^2(\theta/2) + \cos^2\phi} \tag{1}$$

$$\cos\eta = \sin^2\phi\cos\theta + \cos^2\phi \tag{2}$$

$$w = 2b\cdot\sin(\eta/2) \tag{3}$$

$$h = a\cdot\cos(\gamma/2) \tag{4}$$

$$l = 2a\cdot\sin(\gamma/2) \tag{5}$$

$$v = b\cdot\cos(\eta/2) \tag{6}$$

Tessellating the unit cells in the in-plane x and y directions leads to a Miura-ori sheet, such as the ones with 2 by 2 unit cells in Fig. 1(b). To create a 3D structure with geometric gradient, sheets with different sector angles are stacked in the out-of-plane z direction. For instance, joining the two sheets in Fig. 1(b) leads to a two-layer graded structure. By this means, a graded structure with multiple layers can be formed provided that the following geometric constraints are satisfied [12]

$$a_j = \frac{a_1\cos\phi_1}{\cos\phi_j} \tag{7}$$

$$b_j = b_1 \tag{8}$$

$$\theta_j = \cos^{-1}\left(1 - \frac{2\sin^2(\theta_1/2)\sin^2\phi_1}{\sin^2\phi_j}\right) \tag{9}$$

Here a_1, b_1, ϕ_1, θ_1 and a_j, b_j, ϕ_j, θ_j are respectively the geometric parameters in the base layer which is always defined as the layer with the smallest sector angle and denoted as layer 1, and those in an arbitrary layer j ($j = 2,3,\ldots$). Therefore for a multi-layer structure, when the sector angles of all the layers, and the side lengths and folding angle of layer 1 are determined, the geometry of the structure is completely decided. And the overall width W, length L, and height H of the structure can also be obtained

$$W = 2mb_1\cdot\sin(\eta_1/2) \tag{10}$$

$$L = 2na_1\cdot\sin(\gamma_1/2) + b_1\cdot\cos(\eta_1/2) \tag{11}$$

$$H = \sum_{j=1}^{p} a_j\cdot\cos(\gamma_j/2) \tag{12}$$

in which m and n are respectively the numbers of unit cells in a single layer in the x and y directions and p is the number of layers stacked in the z direction. Obviously, if all the layers have identical sector angles, a graded structure reduces to a uniform structure with identical unit cells.

2.2. Self locking

It can be seen from Eq. (9) that due to the variation in sector angles, the folding angles of the layers are also different, and layer 1 with the smallest sector angle ϕ_1 has the largest folding angle θ_1. As a result, a graded structure is only rigid foldable, i.e., the deformation is only caused by rotation of creases while the panels remain rigid, within the range of $0 \le \theta_1 \le 180^\circ$. This point is illustrated by the rigid folding process of the two-layer structure in Fig. 1(c). It can be seen that when $\theta_1 = 180^\circ$, layer 1 is completely flattened whereas layer 2 is still partially folded, and the rigid folding motion of the structure is locked by layer 1, i.e., θ_2 in layer 2 cannot further increase to make this layer flat. After that, the structure has to deform its panels to be further unfolded. The dimensions of a structure at the self locking point can be calculated as follows

$$W_l = 2mb_1\cdot\sin\phi_1 \tag{13}$$

$$L_l = 2na_1 + b_1\cdot\cos\phi_1 \tag{14}$$

$$H_l = a_1\sum_{j=1}^{p}\frac{\sqrt{\sin^2\phi_j - \sin^2\phi_1}}{\cos\phi_j} \tag{15}$$

where the subscript l means locking. And the displacement d in the z direction from the original to the self locking configurations can also be worked out

$$d = H - H_l = a_1\sum_{j=1}^{p}\frac{\cos\phi_1\cos(\gamma_j/2) - \sqrt{\sin^2\phi_j - \sin^2\phi_1}}{\cos\phi_j} \tag{16}$$

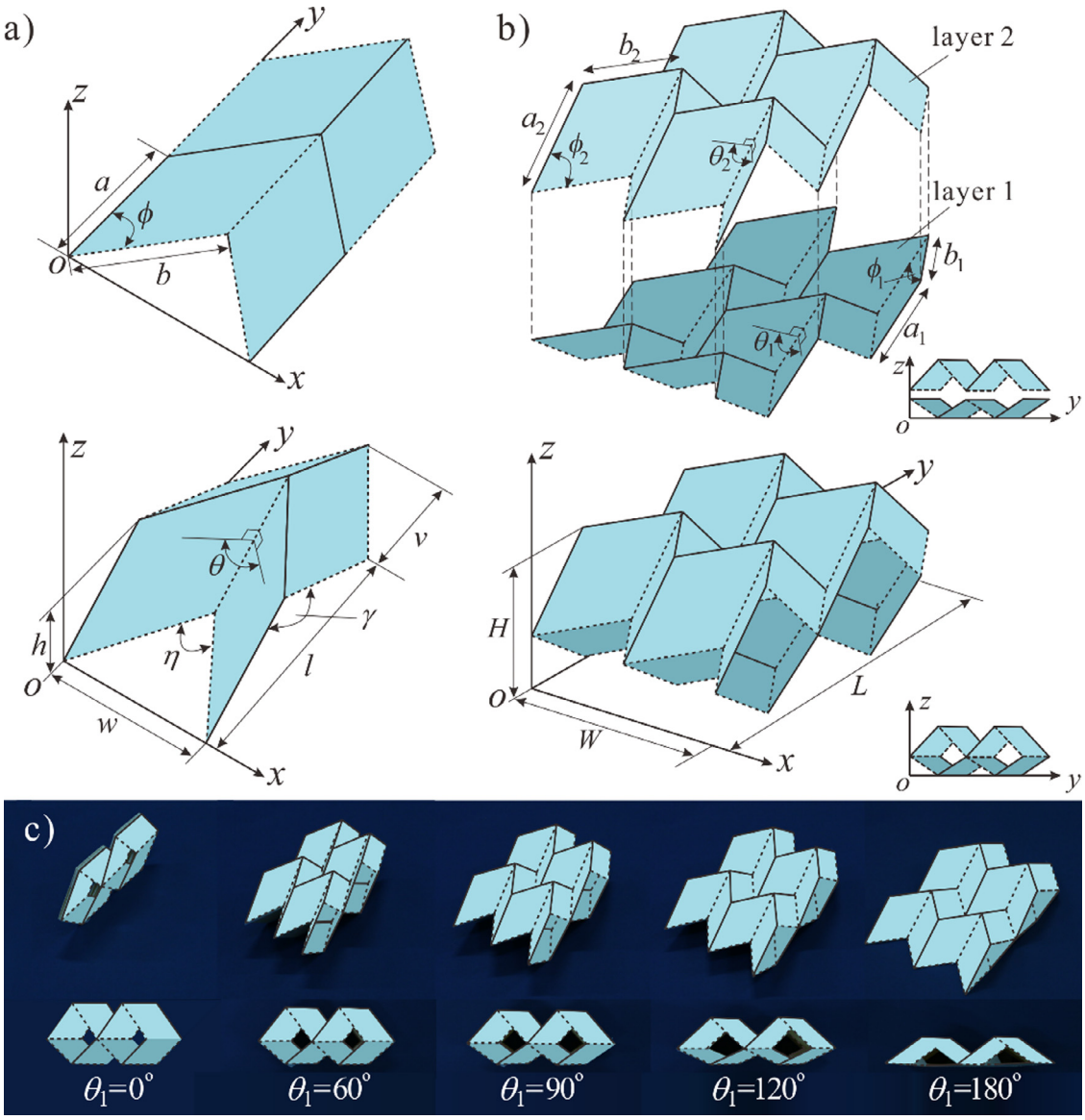

Fig. 1. (a) A unit cell of the Miura-ori pattern in which solid and dashed lines respectively represent mountain and valley creases; (b) A graded origami structure; (c) Rigid folding process of the structure in Fig. 1(b).

Since two deformation stages are involved in the structure, a graded mechanical response could be achieved. To illustrate this concept, sixteen graded origami structures with varying geometries were designed, as well as a uniform one to serve as a benchmark. All the structures were composed of four layers each with 2 by 3 unit cells, illustrated in Fig. 2. The uniform one in Fig. 2(a) had four identical layers with geometric parameters of $\phi_1 = 48^\circ$, $a_1 = 10.57$mm, $b_1 = 10$mm, $\theta_1 = 93.6^\circ$. The overall width, length, and height of the uniform one were $W = 21.67$ mm, $L = 58.88$ mm, and $H = 25.58$ mm, respectively. Regarding to the graded structures, the side lengths and folding angle of layer 1 were so determined to make sure that they had identical overall width and length with the uniform one, whereas those of all the other layers were calculated from Eq. (9). Moreover, the structures were named to reflect the variation in sector angles. For instance, a structure with $\phi_1 = 42^\circ$, $\phi_2 = 46^\circ$, $\phi_3 = 50^\circ$, $\phi_4 = 54^\circ$ was named 42-46-50-54 as shown in Fig. 2(b). The geometries of all the structures are listed in Table 1 together with the numerical results which will be discussed later in the paper.

3. Experimental setup and finite element modelling

3.1. Fabrication

Brass (CuZn40) with a thickness of 0.3 mm was selected in the fabrication of the origami structures. A four-step manufacturing process was adopted as shown in Fig. 3 [38]. First, for each patterned sheet, a series of male and female moulds with gradually reducing folding angles were designed and 3D printed with ABS material through a commercial machine Dimension Elite. For instance, four pairs of moulds shown in Fig. 3(a) with $\theta = 140^\circ$, 120°, 105° and 93.6°, respectively, were constructed for the patterned sheet with $\phi = 48^\circ$ and $\theta = 93.6^\circ$. Second, a flat sheet was successively put in between each pair of moulds in the order of descending folding angles and compressed by an *Instron* 5982 machine to form the pattern (Fig. 3(b)), and then the redundant material from the patterned sheet was removed, see the end product in Fig. 3(c). Subsequently, the patterned sheet was heat treated at 500 °C for 8 min to release residual stress created during folding [39]. And finally, four patterned sheets were glued together to form an origami structure. Com-

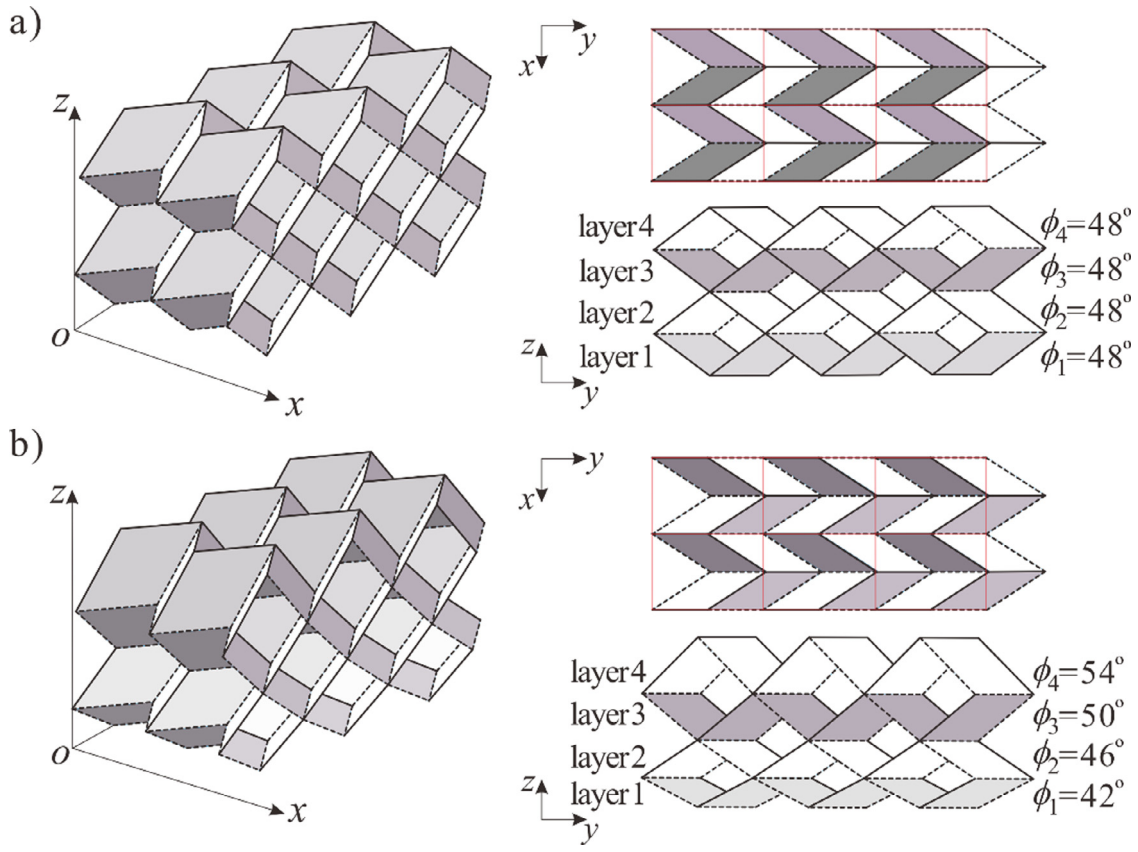

Fig. 2. (a) Model of uniform structure 48-48-48-48; (b) Model of graded structure 42-46-50-54.

Table 1
Geometries of origami structures and numerical results.

Model	a_1 (mm)	θ_1 [°]	H (mm)	Mass (g)	Energy (J)	SEA (J g^{-1})
48-48-48-48	10.57	93.6	25.58	18.84	15.483	0.82
45-47-49-51	10.00	100.0	25.66	18.90	20.533	1.09
43.5-46.5-49.5-52.5	9.75	107.8	25.74	18.99	26.999	1.42
42-46-50-54	9.52	108.1	25.87	19.10	32.284	1.69
40.5-45.5-50.5-55.5	9.30	113.0	26.02	19.25	40.368	2.10
39-45-51-57	9.10	118.8	26.21	19.44	48.735	2.51
42-46-54-50	9.52	108.1	25.87	19.10	31.330	1.64
42-54-46-50	9.52	108.1	25.87	19.10	34.955	1.83
42-50-46-54	9.52	108.1	25.87	19.10	34.547	1.81
42-54-50-46	9.52	108.1	25.87	19.10	36.675	1.92
42-50-54-46	9.52	108.1	25.87	19.10	32.251	1.85
54-42-50-46	9.52	108.1	25.87	19.10	36.118	1.89
50-42-54-46	9.52	108.1	25.87	19.10	36.302	1.90
54-50-42-46	9.52	108.1	25.87	19.10	32.928	1.72
50-54-42-46	9.52	108.1	25.87	19.10	31.553	1.65
54-42-46-50	9.52	108.1	25.87	19.10	35.565	1.86
54-46-42-50	9.52	108.1	25.87	19.10	35.511	1.86

mercially available glue ergo1665NB was adopted. It was determined experimentally that 1.5 g for each specimen was able to maintain structural integrity without noticeably affecting the bending stiffness of the creases. A graded structure 42-46-50-54 constructed in this way is presented in Fig. 3(d) as an instance.

3.2. Experimental setup

To evaluate the mechanical properties of the designs, physical specimens were compressed in the z direction quasi-statically on an *Instron* 5982 testing machine with an upper loading limit of 100 kN. The experimental setup is illustrated in Fig. 4. A specimen stood on top of a fixed plate and compressed by a loading plate which was connected to the load cell, both of which were made of acrylic. An aluminium alloy wall was placed on each side of the specimen, and the spacing L_l between the walls was so chosen that the layer 1 of a specimen was just able to be completely flat but further lateral expansion was prohibited. Note that for the uniform structure, all layers were flattened at the same time, and therefore no walls were added. Displacement control was applied in the experiments and the loading rate was chosen as 5 mm·min^{-1} to avoid dynamic effects. The final compression displacement was chosen as 75% of the structure height to prevent structure densification.

Three specimens of each design were tested, and the specific energy absorption (SEA), defined as the energy absorption per unit mass [40], of each specimen was calculated to study their energy absorption efficiency.

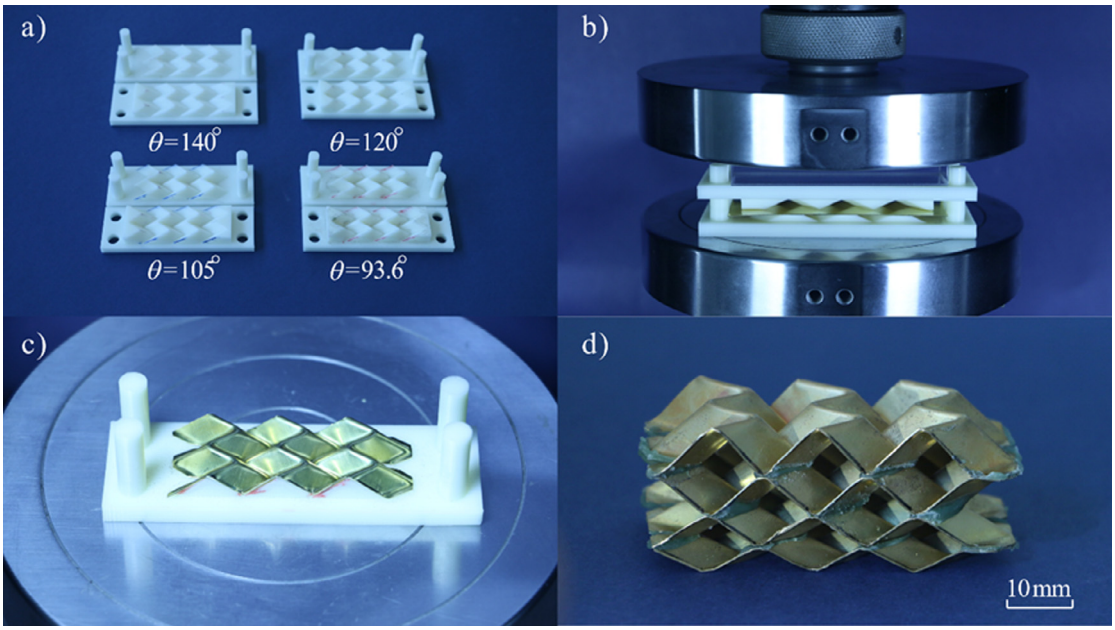

Fig. 3. Fabrication of origami structures. (a) Moulds for stamping patterns on brass sheets; (b) Pattern stamping process using an *Instron*5982 machine; (c) A patterned sheet after stamping; (d) A physical specimen of the graded structure 42-46-50-54.

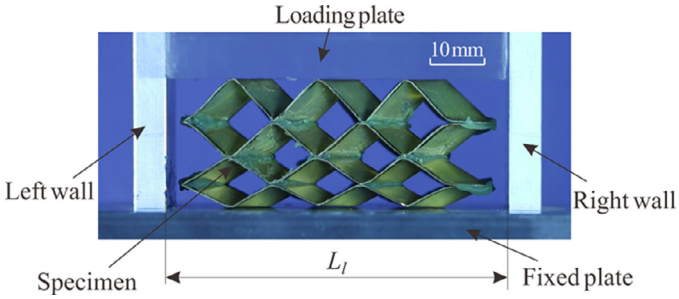

Fig. 4. The experimental setup.

3.3. Finite element modelling

To understand the behaviours of the structures in more details, numerical simulations of the compression experiments were also conducted using commercial finite element code Abaqus/Explicit [41]. The compression scenario was modelled as a model standing on a stationary rigid plate and being compressed by a moving one. The stationary rigid plate was completely fixed in space, whereas all of the degrees of freedom (DOFs) of the moving one were constrained except for the translational DOF in the z direction. Meanwhile, two completely fixed rigid plates were placed on each side of the model at a distance of L_l to simulate the walls in the experiments. A prescribed downward displacement was assigned to the free DOF of the moving rigid plate to control the compression process, and smooth amplitude definition built in Abaqus was assigned to control the loading rate. Different layers in the model were rigidly connected at the folding creases. Four-node shell elements with reduced integration, S4R, were used to mesh the model. Self-contact was employed to simulate the contacts among different parts of the model, and surface-to-surface contact was defined between the model and each rigid plate. Friction was also considered and the friction coefficient μ was taken as 0.25 [9].

The material properties of the brass were characterised through tensile tests of dogbone samples and adopted in the numerical models [42]. The averaged mechanical properties obtained were: Young's modulus $E = 111.1$GPa, yield stress $\sigma_y = 142.0$MPa, tensile strength $\sigma_u = 424.9$MPa, and elongation $\varepsilon_u = 24.2\%$. The density of the material was found to be 8.33 g cm^{-3}.

Convergence tests with respect to mesh density and analysis time, respectively, were also conducted prior to the analysis. Two principles recommended by Abaqus were checked [41], first of all, the ratio of artificial energy to internal energy was below 5% to make sure that hourglassing effect would not significantly affect results; and secondly, the ratio of kinetic energy to internal energy was below 5% during most of the compression process to ensure that dynamic effect could be considered as insignificant. It was found out that a global mesh size of 0.5 mm and an analysis time of 0.02 s yielded satisfactory results.

4. Results and discussions

4.1. Compression of origami structures

The compressions of the uniform structure 48-48-48-48 and the graded one 42-46-50-54 were first studied to demonstrate the graded stiffness induced by geometric design. The deformed configurations at various stages of compression, the corresponding equivalent plastic strain (PEEQ) contour maps drawn on the undeformed shapes, and the force versus displacement curves of the two structures are extracted from the numerical results and compared with the experimental data in Fig. 5. Regarding the numerical models in Fig. 5(a) and (b), the green ones correspond to the deformed configurations, whereas the blue ones correspond to the undeformed configurations where the PEEQ contour maps are drawn on. Figs. 6 and 7 are also presented in the same way. In both cases, a reasonably good match between numerical and experimental data in terms of deformation modes and force versus displacement curves are achieved. Moreover, the difference in SEA between the numerical and averaged experimental results of model 48-48-48-48 is found to be 6.49%, whereas that of model 42-46-50-54 is 6.96%, thereby validating the accuracy of the numerical simulations. In the following discussions the numerical results will be used to reveal more details.

It can be seen from Fig. 5(a) that the uniform model 48-48-48-48 is generally folded in a simultaneous manner. Specifically, the deformation process can be approximately divided into three stages. At stage I with a compression displacement up to 1.3 mm, the structure is predominantly in the elastic range as can be clearly shown from the PEEQ contour

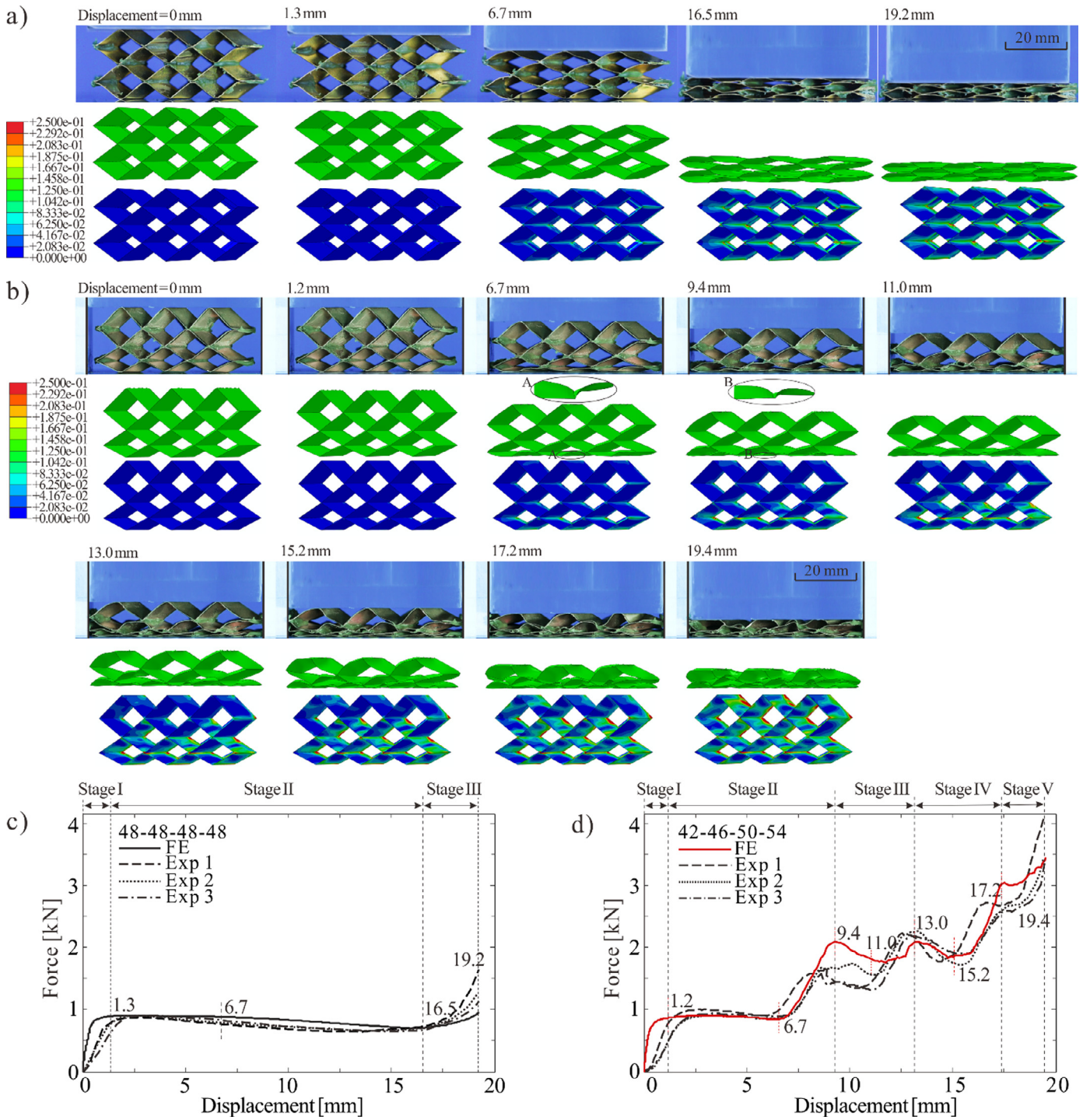

Fig. 5. Experimental and numerical results of the out-of-plane compression of the uniform and graded structures. (a and b) Experimentally and numerically obtained deformation processes of the two structures, respectively. In the experimental parts, the result of 48-48-48-48 corresponds to Exp. 2 in Fig. 5(c), and that of 42-46-50-54 corresponds to Exp. 1 in Fig. 5(d); (c and d) Experimental and numerical force versus displacement curves of the two structures, respectively.

map, and the force increases rapidly with the displacement (Fig. 5(c)). Subsequently at stage II with a displacement of 1.3–16.5 mm, the contour maps show that the creases are bent into plastic range whereas the panels still undergo negligible plastic deformation. Therefore the assumption of rigid folding is satisfied, and the structure can be essentially considered as a mechanism with plastic creases. Correspondingly, a long plateau is formed in the curve. Finally, all the layers are rapidly flattened and squeezed together after the displacement passes 16.5 mm (stage III at 16.5mm-19.2 mm). The model is solidified and becomes very difficult to further compress at this stage, leading to a soaring reaction force. The SEA of the uniform model calculated from the force versus displacement curve is $0.82 J \cdot g^{-1}$.

The graded model 42-46-50-54, different from the uniform one, is mainly deformed in a progressive manner. Roughly five stages can be identified from the deformation process in Fig. 5(b) and the curve in Fig. 5(d). The reaction force still goes up quickly at the beginning (stage I at 0–1.2 mm) and then forms a plateau, referred to as a level 1 plateau. The reason for this plateau to occur, similar to the case of the uniform

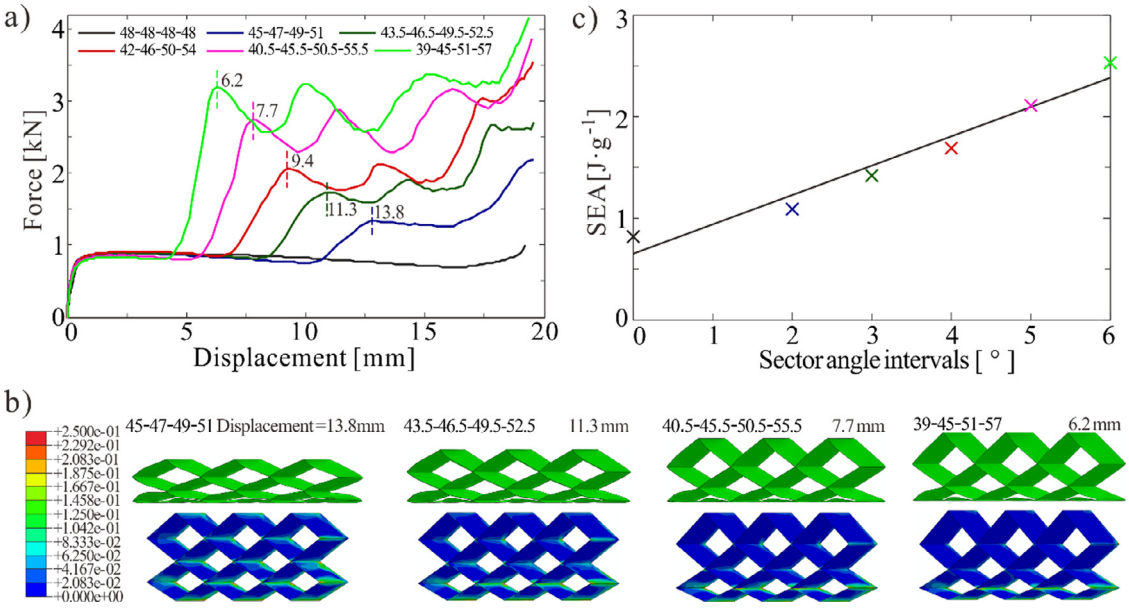

Fig. 6. Effect of sector angle intervals in the graded structure. (a) Numerical force versus displacement curves of the uniform model and five graded ones; (b) Configurations of the numerical models at their respective self locking points; (c) The SEA versus sector angle intervals curve of the numerical models.

model, is that the graded model initially undergoes a rigid folding motion as explained in the previous kinematic analysis. The level 1 plateau continues up to a compression displacement of 6.7 mm, and then increases substantially from 873 N to reach a second peak of 2053 N at a displacement of 9.4 mm. To this point, it has been demonstrated that a graded stiffness is achieved in the structure. To understand the underlying mechanism responsible for the change in stiffness, the deformation process of the model between 6.7 mm and 9.4 mm was taken a close look at. At 6.7 mm, layer 1 is nearly flattened. However, it can be seen from the enlarged crease configuration that since the crease takes the shape of a sharp line instead of a curved surface with a finite width and radius, it is very difficult to be completely unfolded to 180°. As a result, the panels in the neighbourhood have to bend. And when the panels almost bend to flat, further flattening of layer 1 requires stretching more than bending of the panels, which needs a substantially higher force. This transition in deformation mode explains why the force rises at a displacement of 6.7 mm. Meanwhile, the rise in force causes noticeable panel buckling and bending in layer 2, leading to plastic deformation in panels which is clearly demonstrated by the PEEQ contour map at a displacement 9.4 mm. When layer 2 starts to collapse, its load-bearing capacity reaches its maximum. This explains why the force does not rise further at 9.4 mm. Two conclusions can be drawn from the result. First of all, as expected from the kinematic analysis, the flattening of layer 1 locks the rigid folding motion of the structure and generates a sharp increase in reaction force, i.e., self locking is triggered in the structure leading to graded stiffness. Secondly, the theoretical self locking point of the model when $\theta_1 = 180^\circ$ is a displacement of 9.4 mm in the z direction, whereas the numerically obtained one is 6.7 mm. This mismatch is mainly because the difficulty in completely flattening the sharp creases makes self locking appears in advance of the theoretical prediction. Further compression of the structure leads to a successive flattening of layer 2 (stage III at 9.4–13.0 mm) and layer 3 (stage IV at 13.0–17.2 mm), which forms a level 2 plateau in reaction force. Note in the experiments the two local peaks in this range have different magnitudes, whereas those in the numerical simulation are very close. This disparity is mainly caused by the imperfect bonding between layers in the physical specimens, which lowers the first local peak. Finally at stage V from 17.2 mm to 19.4 mm, layer 4 is squeezed, and the force forms a short plateau, referred to as a level 3 plateau, and then increases again until the end of the compression process. Regarding energy absorption, the SEA of the graded structure rises to $1.69\text{J}\cdot\text{g}^{-1}$ owing to large panel bending deformation, 106.10% higher than that of the uniform one.

4.2. Effects of sector angle

Having demonstrated the gradient response and energy absorption of the graded structure, the effect of sector angle variation was further studied through four more numerical models with increased sector angle intervals, namely, 45-47-49-51, 43.5-46.5-49.5-52.5, 40.5-45.5-50.5-55.5, 39-45-51-57. The force versus displacement curves of the models are drawn in Fig. 6(a), and the displacement corresponding to the theoretical self locking point of each model are marked on the curve. The configurations of the models corresponding to the respective self locking points are also presented in Fig. 6(b).

First of all, a level 1 plateau always occurs at the early stage of compression in accordance with the rigid folding motion of a model. Since the models have different rigid folding motion ranges dictated by their geometric parameters, the ranges of the plateaus also vary. But a common feature shared by the models is that the end of the plateau is always in advance of the theoretical self locking point due to the reason mentioned before. The magnitudes of the plateaus, on the other hand, are only marginally affected by the variation of the sector angle. This is because at this stage the force is mainly used to overcome the rotational stiffness of the creases which is the same for all the models.

Secondly, all the curves rise sharply to a second peak after the plateaus, but the larger the sector angle interval, the higher the second peak. The reason is that the increase in sector angle interval causes larger geometric mismatch between layers, which requires a larger force to overcome. And finally, subsequently flattening of layers 2–4 of the models leads to fluctuations and plateaus in their respective curves, but the number of plateaus depends on sector angle intervals. The results show that when the interval is too small as in the cases of 45-47-49-51, or too large as in the case of 39-45-51-57, only two plateaus appear due to that layer 4 tends to deform simultaneously with layer 3, leading to the merging of level 2 and level 3 plateaus. Regarding energy absorption, the SEA of the models listed in Table 1 are drawn with respect to sector angle intervals in Fig. 6(c). A monotonic increase approximately in a linear manner is achieved. And the highest SEA achieved in model 39-45-51-57, $2.51\text{J}\cdot\text{g}^{-1}$, is 306.1% of that of the uniform one. In other words, a threefold increase is realised.

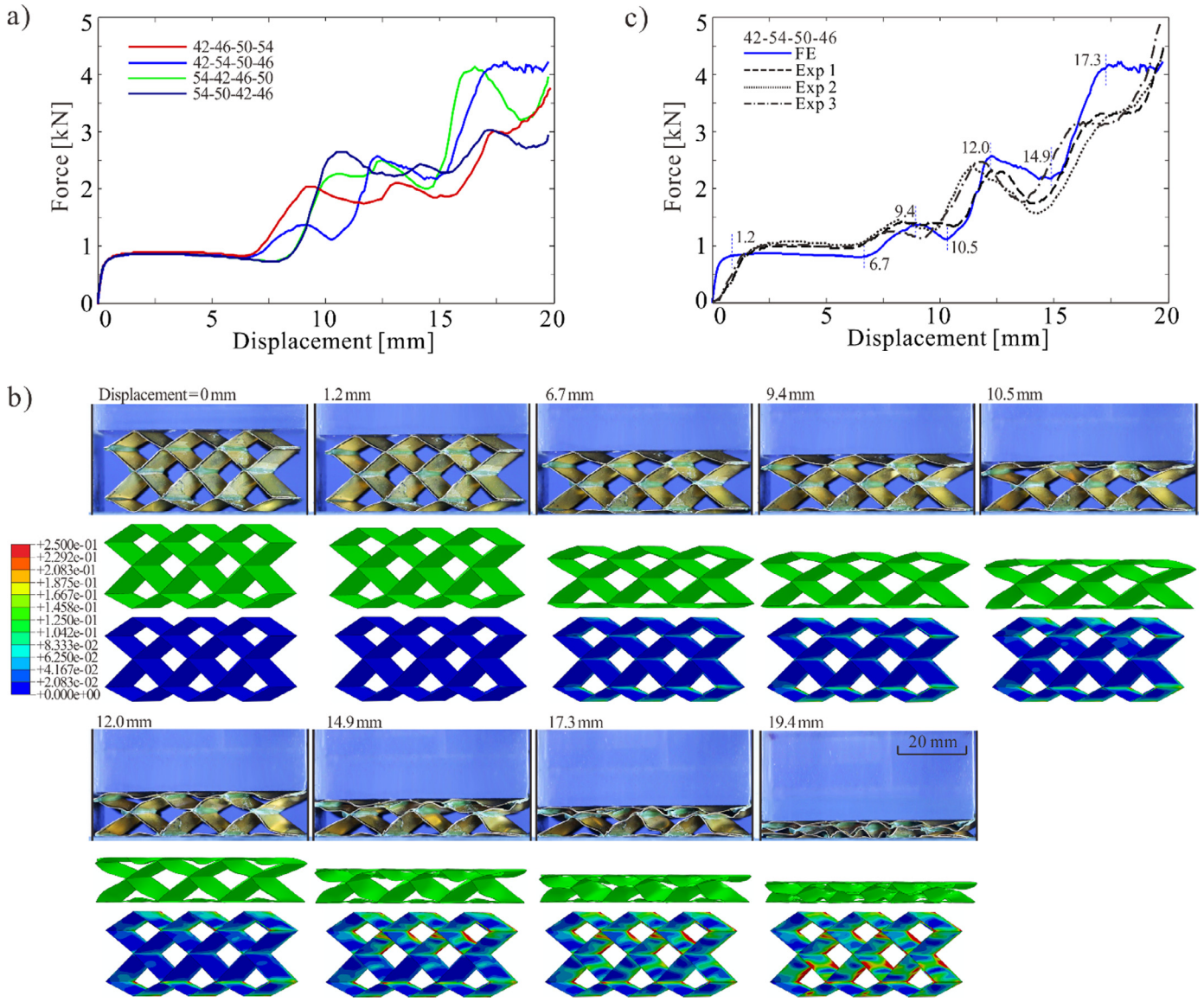

Fig. 7. Effect of layer stacking order in the graded structure. (a) Numerical force versus displacement curves of models, 42-46-50-54, 42-46-54-50, 42-54-50-46, 54-50-42-46; (b) The deformation process of model 42-54-50-46 obtained experimentally and numerically. The experimental result corresponds to Exp. 2 in Fig. 7(c); (c) Experimental and numerical force versus displacement curves of model 42-54-50-46.

4.3. Effects of layer stacking order

To further optimise the geometry of the graded structure, the stacking order of the layers was also changed. Here the model 42-46-50-54 was selected as the baseline, and another 11 variations, namely, 42-46-54-50, 42-50-46-54, 42-54-46-50, 42-54-50-46, 42-50-54-46, 50-42-54-46, 50-54-42-46, 54-42-46-50, 54-42-50-46, 54-46-42-50, and 54-50-42-46, were built and analysed numerically. The reaction force versus displacement curves of all the models were extracted from the numerical results, and their SEA were also calculated and listed in Table 1.

The results indicate that changing layer stacking order affects both the curve shape and energy absorption of a graded structure. Three representative models, 42-54-50-46, 54-42-46-50, 54-50-42-46 which were found to generate force curves with different number of plateaus, are presented in Fig. 7(a) together with that of the baseline 42-46-50-54. It can be seen that by varying layer stacking order, two-level, three-level, and four-level graded stiffness are successfully created. In terms of energy absorption, model 42-54-50-46 with four-level graded stiffness has the largest SEA of $1.92 J \cdot g^{-1}$, 13.61% higher than that of the baseline 42-46-50-54, and 134.15% higher than that of the uniform one 48-48-48-48. Notice that despite the optimal stacking order being obtained, the relationship between stacking order and the mechanical properties of the structure is not fully understood, which requires further investigation.

Having determined the optimal stacking order, three physical specimens of model 42-54-50-46 were built using the same technique as illustrated before and compressed quasi-statically. The deformation process of the physical specimen is presented in Fig. 7(b), which excellently replicates what is obtained numerically. Moreover, the experimental and numerical force versus displacement curves drawn in Fig. 7(c) also matches reasonably well in shape, with a SEA difference of 9.71% being achieved.

5. Conclusion

In conclusion, we have designed a graded structure based on the Miura-ori pattern to achieve both graded stiffness and superior energy absorption performance. Specifically, we have found that the new structure undergoes both mechanism mode where the deformation is concen-

trated on the creases and structural mode where both creases and panels are deformed, and the transfer from the first to the second is realised through an intrinsic self locking geometric constraint. We have demonstrated both experimentally and numerically that the graded structure is able to generate up to four-level graded stiffness which can be tuned through its geometric parameters. Moreover, the graded structure has superior energy absorption efficiency, with a threefold increase in SEA being achieved in the optimal case in comparison with uniform structures. The design proposed here is purely geometric, and therefore can be readily used to create origami mechanical metamaterials provided that the unit sizes are scaled down. Our work provides a new avenue in the design of origami structures and mechanical metamaterials that are tunable and adaptable to external loads.

Acknowledgements

Y.C. acknowledges the support of the National Natural Science Foundation of China (Projects 51290293 and 51422506) and the Ministry of Science and Technology of China (Project 2014DFA70710), and J.M. acknowledges the support of the National Natural Science Foundation of China (Project 51575377).

References

[1] Miura K. presented at Inst. Space. Astron. Sci. Rep. No. 618, Tokyo, Japan, November 1985.
[2] Gardner JP, Mather JC, Clampin M, Doyon R, Greenhouse MA, Hammel HB, et al. The James Webb space telescope. Space Sci Rev 2006;123:485–606.
[3] Kuribayashi K, Tsuchiya K, You Z, Tomus D, Umemoto M, Ito T, et al. Self-deployable origami stent grafts as a biomedical application of Ni-rich TiNi shape memory alloy foil. Mater Sci Eng A 2006;419(1-2):131–7. doi:10.1016/j.msea.2005.12.016.
[4] Ma J, You Z. Energy absorption of thin-walled square tubes with a prefolded origami pattern—part I: geometry and numerical simulation. J Appl Mech 2013;81(1):11003. doi:10.1115/1.4024405.
[5] Zhou C, Wang B, Ma J, You Z. Dynamic axial crushing of origami crash boxes. Int J Mech Sci 2016;118:1–12. doi:10.1016/j.ijmecsci.2016.09.001.
[6] Wang B, Zhou C. The imperfection-sensitivity of origami crash boxes. Int J Mech Sci 2017;121(November 2016):58–66. doi:10.1016/j.ijmecsci.2016.11.027.
[7] Ma J, Hou D, Chen Y, You Z. Quasi-static axial crushing of thin-walled tubes with a kite-shape rigid origami pattern: numerical simulation. Thin-Walled Struct 2016;100:38–47. doi:10.1016/j.tws.2015.11.023.
[8] Yang Y, Nara C, Hagiwara I. Energy absorption characteristics of pairing origami structure. In: Proc dyn des conf; 2016. p. 526. doi:10.1299/jsmedmc.2016.526.
[9] Yang K, Xu S, Shen J, Zhou S, Xie YM. Energy absorption of thin-walled tubes with pre-folded origami patterns: Numerical simulation and experimental verification. Thin-Walled Struct 2016;103:33–44. doi:10.1016/j.tws.2016.02.007.
[10] Wu S, Li G, Sun G, Wu X, Li Q. Crashworthiness analysis and optimization of sinusoidal corrugation tube. Thin-Walled Struct 2016;105:121–34. doi:10.1016/j.tws.2016.03.029.
[11] Fathers RK, Gattas JM, You Z. Quasi-static crushing of eggbox, cube, and modified cube foldcore sandwich structures. Int J Mech Sci 2015;101-102:421–8. doi:10.1016/j.ijmecsci.2015.08.013.
[12] Schenk M, Guest SD. Geometry of Miura-folded metamaterials. Proc Natl Acad Sci 2013;110(9):3276–3281. doi:10.1073/pnas.1217998110.
[13] Lv C, Krishnaraju D, Konjevod G, Yu H, Jiang H. Origami based mechanical metamaterials. Sci Rep 2014;4:5979 (August). doi:10.1038/srep05979.
[14] Wei ZY, Guo ZV, Dudte L, Liang HY, Mahadevan L. Geometric mechanics of periodic pleated origami. Phys Rev Lett 2013;110(21):1–5. doi:10.1103/PhysRevLett.110.215501.
[15] Zhou X, Zang S, You Z. Origami mechanical metamaterials based on the Miura-derivative fold patterns. Proc R Soc A Math Phys Eng Sci 2016;472(2191):20160361. doi:10.1098/rspa.2016.0361.
[16] Kamrava S, Mousanezhad D, Ebrahimi H, Ghosh R, Vaziri A. Origami-based cellular metamaterial with auxetic, bistable, and self-locking properties. Sci Rep 2017;7:46046. doi:10.1038/srep46046.
[17] Yasuda H, Yang J. Reentrant origami-based metamaterials with negative Poisson's ratio and bistability. Phys Rev Lett 2015;114(18):1–5. doi:10.1103/PhysRevLett.114.185502.
[18] Silverberg JL, Evans AA, McLeod L, Hayward RC, Hull T, Santangelo CD, et al. Using origami design principles to fold reprogrammable mechanical metamaterials. Science 2014;345(6197):647–50. doi:10.1126/science.1252876.
[19] Virk K, Monti A, Trehard T, Marsh M, Hazra K, Boba K, et al. SILICOMB PEEK Kirigami cellular structures: mechanical response and energy dissipation through zero and negative stiffness. Smart Mater Struct 2013;22(8):84014. doi:10.1088/0964-1726/22/8/084014.
[20] Filipov ET, Tachi T, Paulino GH. Origami tubes assembled into stiff, yet reconfigurable structures and metamaterials. Proc Natl Acad Sci USA 2015;112(40):12321–6. doi:10.1073/pnas.1509465112.
[21] Eidini M, Paulino GH. Unraveling metamaterial properties in zigzag-base folded sheets. Sci Adv 2015;1(8) e1500224-e1500224. doi:10.1126/sciadv.1500224.
[22] Silverberg JL, Na JH, Evans AA, Liu B, Hull TC, Santangelo CD, et al. Origami structures with a critical transition to bistability arising from hidden degrees of freedom. Nat Mater 2015;14(4):389–93. doi:10.1038/nmat4232.
[23] Gattas JM, You Z. Geometric assembly of rigid-foldable morphing sandwich structures. Eng Struct 2015;94:149–59. doi:10.1016/j.engstruct.2015.03.019.
[24] Fang H, Wang KW, Li S. Asymmetric energy barrier and mechanical diode effect from folding multi-stable stacked-origami. Extreme Mech Lett 2017;17:7–15.
[25] Xie R, Li J, Chen Y. The graded origami structures. ASME 2015 international design engineering technical conferences and computers and information in engineering conference Boston, Massachusetts; 2015. USA.
[26] Schuster PJ. Current trends in bumper design for pedestrian impact. Sae 2006-01-0464. SAE international; 2006. doi:10.4271/2006-01-0464.
[27] Davoodi MM, Sapuan SM, Aidy A, Osman NAA, Oshkour AA, Abas WABW. Development process of new bumper beam for passenger car: a review. Mater Des 2012;40:304–13. doi:10.1016/j.matdes.2012.03.060.
[28] Bartha T. Non-lethal weapons against persons. AARMS 2003;2(2):293–305.
[29] Amada S. Hierarchical functionally gradient structures of bamboo barley, and corn. Mrs Bull 1995;20(1):35–6. doi:10.1557/S0883769400048909.
[30] Claussen KU, Scheibel T, Schmidt HW, Giesa R. Polymer gradient materials: can nature teach us new tricks? Macromol Mater Eng 2012;297(10):938–57. doi:10.1002/mame.201200032.
[31] Jha DK, Kant T, Singh RK. A critical review of recent research on functionally graded plates. Comp Str 2013;96:833–49. doi:10.1016/j.compstruct.2012.09.001.
[32] Cui L, Kiernan S, Gilchrist MD. Designing the energy absorption capacity of functionally graded foam materials. Mater Sci Eng A 2009;507(1-2):215–25. doi:10.1016/j.msea.2008.12.011.
[33] Sun G, Li G, Hou S. Crashworthiness design for functionally graded foam-filled thin-walled structures. Mater Sci Eng A 2010;527:1911–19. doi:10.1016/j.msea.2009.11.022.
[34] Omid M, Hashem G. Optimal shape design of functionally graded thickness inversion tubes subjected to oblique loading. Struct Multidisc Optim 2017;56:587–601. doi:10.1007/s00158-017-1776-6.
[35] Sun G, Xu F, Li G, Li Q. Crashing analysis and multiobjective optimization for thin-walled structures with functionally graded thickness. Int J Impact Eng 2014;64:62–74. doi:10.1016/j.ijimpeng.2013.10.004.
[36] Li G, Zhang Z, Sun G, Huang X, Li Q. Comparison of functionally-graded structures under multiple loading angles. Thin-Walled Struct 2015;94:334–47. doi:10.1016/j.tws.2015.04.030.
[37] Gattas JM, Wu W, You Z. Miura-base rigid origami: parameterizations of first-level derivative and piecewise geometries. J Mech Des 2013;135:111011.
[38] Gattas JM, You Z. Quasi-static impact of indented foldcores. Int J Impact Eng 2014;73:15–29. doi:10.1016/j.ijimpeng.2014.06.001.
[39] Ding H, Wu Q, Ma L. Deformation behaviour in α/β two-phase super-plastic brass. J Mater Sci 1992;27:607–10.
[40] Lu G, Yu T. Energy absorption of structures and materials. Boca Raton, FL, USA: CRC; 2003.
[41] Abaqus Analysisi User's Manaul, Abaqus documentation version 6.14-1, dassault systems SIMULA Corp. Providence, RI, USA, 2014.
[42] International Organization for Standardization, Metallic materials—tensile testing—part 1: method of test at room temperature, ISO 6892-1:2016, International Organization for Standardization, Geneva.